Time Evolving Matrix Product States

By

Afroze Zehra

Department of Physics

Quaid-i-Azam University, Islamabad, Pakistan

(2020-2022)

Time Evolving Matrix Product States

By

Afroze Zehra

Department of Physics
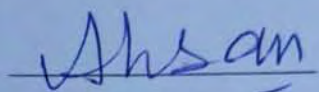
Quaid-i-Azam University, Islamabad, Pakistan

(2020-2022)

A DISSERTATION SUBMITTED IN PARTIAL FULFILLMENT OF THE
REQUIREMENTS FOR THE DEGREE OF MASTERS OF
PHILOSOPHY IN PHYSICS AT THE QUAID-I-AZAM UNIVERSITY,
ISLAMABAD 45320, PAKISTAN. AUGUST, 2022.

RESEARCH COMPLETION CERTIFICATE

Certified that the research work contained in the thesis titled Time Evolving Matrix Product States has been carried out and completed by Ms. Afroze Zehra Roll No. 02182013007 under my supervision.
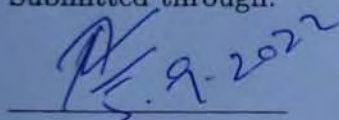
Supervised by:

Dr. Ahsan Zeb

Department of Physics

Quaid-i-Azam University Islamabad

Submitted through:

Prof. Dr. Nawazish Ali Khan

Chairperson

Department of Physics

Quaid-i-Azam University Islamabad

DECLARATION

I, Ms. **Afroze Zehra** Roll No.**02182013007**, student of M.Phil., in the subject of Physics session 2020-22, hereby declare that the matter printed in the thesis titled **"Time Evolving Matrix Product States"** is my review work and has not been printed, published or submitted as research work, thesis or publication in any form in any University, Research Institution etc. in Pakistan.

Dated 19$^{\text{th}}$ August, 2022

RESEARCH COMPLETION CERTIFICATE

Certified that the research work contained in the thesis titled Time Evolving Matrix Product States has been carried out and completed by Ms. Afroze Zehra Roll No. 02182013007 under my supervision.

Supervised by:

_____

Dr. Ahsan Zeb

Department of Physics

Quaid-i-Azam University Islamabad

Submitted through:

_____

Prof. Dr. Kashif Sabeeh

Chairperson

Department of Physics

Quaid-i-Azam University Islamabad

DEDICATION

To my adorable little son, Muhammad Raza,

my sweet laddu.

Abstract

Studying non-Markovian open quantum systems coupled strongly with their environments is essential for the development of future quantum technologies. Such systems are ubiquitous in real life but quite poorly understood. Here we develop a numerical approach to solve open quantum system coupled to a harmonic environment based on Feynman Vernon Influence Functional. The history of the system evolution is stored in an augmented density tensor (ADT) in order to study the non-Markovian behaviour. The ADT scheme, however, cannot account for non-Markovian effects that go far back in time. Here we represent the influence functional and the ADT as time-evolving matrix product operators (TEMPO) and states (TEMPS), respectively. At each time step, the matrix product operator and state are contracted to give the time-evolved state which is decomposed using singular value decomposition and truncation. This method is very efficient and works for different coupling regimes. We demonstrate the robustness of the TEMPO algorithm by examining the phonon-induced damping of Rabi Oscillations in semiconductor Quantum Dots coupled to a cavity for different phonon-exciton couplings. The decay rates of Rabi Oscillations at different temperatures are also compared.

Acknowledgements

Thanks to Allah, the most kind and the most merciful. First and foremost, I would like to thank my supervisor, Dr Ahsan Zeb, whose support and guidance made it possible for me to complete this task smoothly along with the fulfillment of my family duties. The detailed discussions with him, his expert advice and in-depth analysis were invaluable in developing a sound understanding of the core concepts.

Heartiest thanks to all the teachers and elders who have played a role in my development, and believed in me.

I am forever indebted to my family especially my parents, who raised me well, and have always supported and loved me unconditionally, and my sisters, whose never ending criticisms and the high expectations from me always push me to do better. My special thanks to my parents-in-law especially my mother-in-law, for if it was not for her unwavering support, I would not have managed to complete my degree. Lastly, my dear husband whose love and support is an assurance of a promising and bright future, and my little son, whose raucous is always a pleasant disruption in my work.

Contents

1

List of Figures

Chapter 1

Introduction

Quantum systems that interact with their environments are referred to as *open quantum systems* (OQS). Their interaction with the environment results in phenomena such as decoherence and dissipation. These systems are ubiquitous in nature. In plants, the phononic environment created by the vibrations of proteins affects the rate of energy transfer in photosynthesis [1, 2]. The problem of a quantum system interacting with its environment has been long-studied in the area of molecular physics. Furthermore, extensive research is being carried out in solid state physics and quantum optics [3]. Semiconductor systems such as quantum dots not only possess rich and interesting physics, but also have wide industrial applications [4]. Now, with the rapid emergence of quantum technologies, it has become increasingly important to study the OQSs in order to further improve our understanding of nature and accelerate the development in this industry.

The OQSs can be sub-divided as Markovian and non-Markovian sytems [5]. In situations where the coupling between the system and environment is weak, we can assume that the environment is *memoryless*. This means that after the interaction, the environment bounces back to its equilibrium state

instantaneously, thus forgetting that it ever interacted with the system. This is called Markov approximation. For this approximation to be valid, the relaxation time of the system must be long as compared to the bath correlation time. Markovian systems can be solved exactly using Born-Markov master equations.

As we go beyond the weak-coupling regime, the environment can no longer be assumed to be memoryless and the system's history must be taken into account. In such situations, the system and bath timescales are of the same order and information can back-flow from the environment into the system. This results in interesting non-Markovian dynamics [6, 7]. Hence, it becomes crucial to find an accurate description of OQS strongly coupled to their environment in order to fully understand how quantum systems dissipate energy and lose their coherence.

Several perturbative approaches using master equations exist for studying non-Markovian dynamics [5, 6]. However, these methods are limited to strict parameter regimes. We need more general methods to solve a larger variety of problems. Here we introduce a non-pertubative method that uses Feynman path integral formulation of OQS. To improve efficiency, the method is then implemented using tensor networks, in particular, matrix product states (MPS).

This scheme is primarily developed for a few level system linearly coupled to a bath comprising of an infinite set of harmonic oscillators. Harmonic baths can model a number of environments such as photonic and phononic environments.

The method involves integrating out the bath degrees of freedom to obtain a *discretized Feynman influence functional* that carries all the effects of the bath on the system and acts only on the reduced system states. Further-

more, in order to keep track of the system's history, we use an *augmented density tensor* (ADT) to represent the state of the system at time t. The influence functional couples the current evolution to the history and captures the non-Markovian dynamics.

As the system evolves, the history of the system lengthens and the ADT quickly grows to the point where it becomes unphysical to store it. To overcome this problem, we assume that the bath has a finite memory. This approximation known as the *finite memory approximation* allows us to propagate the ADT containing only previous K timesteps. For efficient implementation of the algorithm, the ADT is represented as Matrix Product States (MPS) and the influence functional is represented as Matrix Product Operators (MPO). For this reason, the method is named ", called Time-Evolving Matrix Product Operators (TEMPO)" [8, 7]. The ADT is then evolved using standard MPS/MPO methods.

The layout of the thesis is as follows. In Chapter 2, we provide the necessary background and discuss the TEMPO algorithm in detail. In Chapter 3, we study the physics of a quantum dot coupled to a cavity using the method developed in Chapter 2. In Chapter 4, we conclude the discussion with a short summary of our results and a brief discussion on more applications of the algorithm.

Chapter 2

Method

Consider a system with a few degrees of freedom coupled linearly to a harmonic bath. The Hamiltonian of the bath is

$$H_b = \sum_i \omega_i \hat{a}_i^\dagger \hat{a}_i, \tag{2.1}$$

where ω_i is the frequency and $\hat{a}_i^\dagger (\hat{a}_i)$ is the creation (annihilation) operator of the ith bath mode. For a spatially large environment, it is a good approximation to take system-bath coupling as linear in bath coordinates. The Hamiltonian for the system-bath interaction reads

$$H_{s-b} = \sum_i \hat{s}(g_i \hat{a}_i + g_i^* \hat{a}_i^\dagger), \tag{2.2}$$

where $\hat{s}$ is the system operator that couples to bath mode i with coupling strength, g_i.

The total Hamiltonian is written as

$$H = H_0 + \sum_i \hat{s}(g_i \hat{a}_i + g_i^* \hat{a}_i^\dagger) + \sum_i \omega_i \hat{a}_i^\dagger \hat{a}_i, \tag{2.3}$$

$$= H_0 + H_B \tag{2.4}$$

where H_0 is the free system Hamiltonian and H_B consists of the bath Hamiltonian and the system-bath interaction.

2.1 Feynman-Vernon Influence Functional

In this section, we derive an analytic expression for the Feynman-Vernon influence functional. It is based on Feynman's path integral formalism (see Appendix A for a brief introduction) [9, 10].
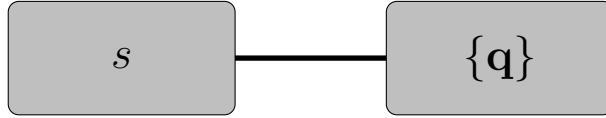

Figure 2.1: Schematic diagram of a system s linearly coupled to the environment oscillators with coordinates $\mathbf{q} = \{q_1, q_2, \dots\}$

For an open system with coordinates s coupled linearly to an infinite set of harmonic oscillators $\mathbf{q} = \{q_i\} = \{q_1, q_2, \dots\}$ as schematized in Fig. 2.1 [11], the total density matrix is given by

$$\rho_t(t) \equiv \rho_t(s, s', \mathbf{q}, \mathbf{q}', t). \tag{2.5}$$

We assume that the system and bath are initially uncorrelated.

$$\rho_t(t_i) = \rho(t_i) \otimes \rho_B(t_i) \tag{2.6}$$

Drawing from the expression derived in Eq. (A.7) and the initial condition Eq. (2.6), we write the matrix element of the time-evolved total density matrix as

$$\langle s_f, \mathbf{q}_f | \rho_t(t_f) | s'_f, \mathbf{q}'_f \rangle = \int ds_i ds'_i d\mathbf{q}_i d\mathbf{q}'_i \mathbf{J}(s_f, s'_f, \mathbf{q}_f, \mathbf{q}'_f, t_f; s_i, s'_i, \mathbf{q}_i, \mathbf{q}'_i, t_i)$$
$$\times \langle s_i | \rho(t_i) | s'_i \rangle \langle \mathbf{q}_i | \rho_B(t_i) | \mathbf{q}'_i \rangle. \tag{2.7}$$

For clarity, we write the above expression compactly as

$$\langle \rho_t(t_f) \rangle = \int ds_i ds'_i d\mathbf{q}_i d\mathbf{q}'_i \mathbf{J}(t_f | t_i) \langle \rho(t_i) \rangle \langle \rho_B(t_i) \rangle, \tag{2.8}$$

7

where

$$\mathbf{J}(t_i; t_f) = \int_i^f \mathcal{D}[s]\mathcal{D}[s']\mathcal{D}[\mathbf{q}]\mathcal{D}[\mathbf{q}']\exp\left(iS[s,\mathbf{q}] - iS[s',\mathbf{q}']\right). \qquad (2.9)$$

Here, $S[s,\mathbf{q}]$ is the total action which can be written as

$$S[s,\mathbf{q}] = S_0[s] + S_B[s,\mathbf{q}], \qquad (2.10)$$

where $S_0[s]$ is the action for the open system and $S_B[s,\mathbf{q}]$ is the action for the bath and the system-bath interaction. Inserting these in the above expression and separating out the system and bath terms, we get

$$\mathbf{J}(t_i; t_f) = \int_i^f \mathcal{D}[s]\mathcal{D}[s'](iS_0[s] - iS_0[s']) \int_i^f \mathcal{D}[\mathbf{q}]\mathcal{D}[\mathbf{q}']\exp\left(iS_B[s,\mathbf{q}] - iS_B[s',\mathbf{q}']\right). \tag{2.11}$$

Defining the first integral in Eq. (2.11) as

$$\mathcal{F}[s,s'] = \int_i^f \mathcal{D}[s]\mathcal{D}[s']\exp\left(iS_0[s] - iS_0[s']\right) \qquad (2.12)$$

The functional $\mathcal{F}$ constitutes the free part of the evolution. That is, it contains the information about the evolution of the system as if there was no environment present.

Now the propagator may be written as

$$\mathbf{J}(t_i; t_f) = \mathcal{F}[s,s'] \int_i^f \mathcal{D}[\mathbf{q}]\mathcal{D}[\mathbf{q}']\exp\left(iS_B[s,\mathbf{q}] - iS_B[s',\mathbf{q}']\right) \qquad (2.13)$$

Since we are only interested in the evolution of the open system, we trace out the bath degrees of freedom to obtain an expression for the reduced density matrix, ρ [11].

$$\rho(t) \equiv \rho(s,s',t) = \int d\mathbf{q}[\rho_t(t)]_{\mathbf{q}=\mathbf{q}'} \qquad (2.14)$$

The matrix element of the time-evolved reduced density matrix is given by

$$\langle s_f| \rho(t) |s_f'\rangle = \int d\mathbf{q}_f[\langle s_f,\mathbf{q}_f| \rho_t(t) |s_f',\mathbf{q}_f'\rangle]_{\mathbf{q}_f=\mathbf{q}_f'} \qquad (2.15)$$

$$= \int d\mathbf{q}_f \langle s_f,\mathbf{q}_f| \rho_t(t) |s_f',\mathbf{q}_f\rangle \qquad (2.16)$$

8

In path integral representation,

$$\langle \rho(t_f) \rangle = \int ds_i ds_i' \mathbf{W}(t_f; t_i) \langle \rho(t_i) \rangle \qquad (2.17)$$

where

$$\mathbf{W}(t_f; t_i) = \int d\mathbf{q}_f d\mathbf{q}_i d\mathbf{q}_i' \mathbf{J}(t_f; t_i) \rho_B(t_i). \qquad (2.18)$$

Using the expression for $\mathbf{J}$ in Eq. (2.13) in the above equation and separating out the system and bath terms, we get

$$\mathbf{W}(s_f, s_f', t_f; s_i, s_i', t_i) = \mathcal{F}[s, s'] \mathcal{I}[s, s'] \qquad (2.19)$$

where

$$\mathcal{I}[s, s'] = \int_i^f d\mathbf{q}_f d\mathbf{q}_i d\mathbf{q}_i' \int_i^f \mathcal{D}[\mathbf{q}] \mathcal{D}[\mathbf{q}'] \exp\left(iS_B[s, \mathbf{q}] - iS_B[s', \mathbf{q}']\right) \rho_B(t_i). \qquad (2.20)$$

Note that for $\mathcal{I}[s, s'] = 1$, W describes the evolution of a free system. This illustrates that the functional $\mathcal{I}[s, s']$ contains complete information regarding the influence of the bath on the system. $\mathcal{I}[s, s']$ is the *Feynman-Vernon influence functional* [12, 13].

Here we have assumed that the bath is harmonic, couples linearly to the system and is, initially, in thermal equilibrium. Carrying out all the integrations, we get the following expression for $\mathcal{I}$,

$$\mathcal{I}[s, s'] = \Phi, \qquad (2.21)$$

where Φ, known as the *phase influence functional* is given by

$$\Phi = -\int_0^t \int_0^{t'} dt'' dt' \left(s(t') - s'(t')\right) \left(C(t' - t'')s(t') - C(t - t')s'(t')\right), \qquad (2.22)$$

where C is the *bath autocorrelation function* for the spectral density of bath, $J(\omega) = \sum_i |g_i|^2 \delta(\omega_i - \omega)$ at temperature, T

$$C(t) = \frac{1}{\pi} \int_0^\infty J(\omega) \left(\coth\left(\frac{\omega}{2T}\right) \cos\omega t - i\sin\omega t \right) d\omega. \qquad (2.23)$$

Note that the bath Hamiltonian, H_B is completely characterized by the system operator, $\hat{s}$, coupling strength, g and bath mode frequency, ω.

In order to make the influence functional computable, we must discretize it. This is achieved by discretizing the Feynman paths $\{s(t), s'(t)\}$ by splitting them into intervals of equal duration.

$$\{s(t), s'(t)\} = \{s_k^+, s_k^-\}_{k=0}^N, \qquad (2.24)$$

such that each $s_k^\pm$ is constant w.r.t. time [14]. Here k is a timestep and N is the total number of timesteps.

Now the phase influence functional reads

$$\Phi[s, s'] = -\sum_{k=1}^N \sum_{k'=1}^k (s_k^+ - s_k^-)(\eta_{k-k'} \, s_{k'}^+ - \eta_{k-k'} \, s_{k'}^-), \qquad (2.25)$$

where the coefficients $\eta_{k-k'}$ are given by

$$\eta_{k-k'} = \begin{cases} \int_{t_{k-1}}^{t_k} \int_{t_{k'-1}}^{t_{k'}} C(t' - t'')dt''dt' & k \neq k' \\ \int_{t_{k-1}}^{t_k} \int_{t_{k-1}}^{t'} C(t' - t'')dt''dt' & k = k' \end{cases} \qquad (2.26)$$

We may write the discretized influence functional as a product of influence functions, $I_{k'}$ [8],

$$\mathcal{I}[s, s'] = \prod_{k=1}^N \prod_{k'=1}^k I_{k'}(s, s') \qquad (2.27)$$

where

$$I_{k'}(s, s') = \exp\left(\Phi_{k'}(s, s')\right) \qquad (2.28)$$

10

2.2 Discretized Influence Functional in Liouville Space

The state of a system is completely described by the density operator, $\hat{\rho}$. In a d-dimensional Hilbert space, the density operator is a $d \times d$ matrix. To simplify our notation, we work in Liouville space. In this space, the density operator is represented by a vector with d^2 elements and written as $|\rho\rangle\rangle$. The propagator that evolves these vectors is known as a *superoperator* and is represented by a $d^2 \times d^2$ matrix.

The reduced density operator for initially uncorrelated system and bath is then written as

$$|\rho(t)\rangle\rangle = Tr_B\{|\rho(0)\rangle\rangle \, |\rho_B(0)\rangle\rangle\} \tag{2.29}$$

For a generic reduced system with eigenvalue equations, $\hat{s}\,|s^+\rangle = s^+\,|s^+\rangle$ and $\hat{s}\,|s^-\rangle = s^-\,|s^-\rangle$, the density operator can be written as a linear combination of system eigenstates

$$\hat{\rho} = \sum_S \rho_S |S\rangle\rangle \equiv |\rho\rangle\rangle, \tag{2.30}$$

where $|S\rangle\rangle$ are the system eigenstates and the sum over S runs over the d^2 pairs of $\{s^+, s^-\}$. Similarly, we can write the bath density operator in terms of the bath eigenstates, $|B\rangle\rangle$.

The time evolution of the density operator is represented as

$$|\rho(t)\rangle\rangle = e^{\mathcal{L}t}|\rho(0)\rangle\rangle, \tag{2.31}$$

where $\mathcal{L} = \frac{1}{\hbar}[H, \rho]$ is the Liouvillian and $e^{\mathcal{L}t}$ is a superoperator. The evolution generated by $\mathcal{L} = \mathcal{L}_0 + \mathcal{L}_B$ in Liouville space corresponds exactly with that caused by $H = H_0 + H_B$ in Hilbert space.

To obtain a discretized influence functional, we factorize the propagator $e^{\mathcal{L}t}$

$$\hat{\rho} = \begin{pmatrix} \rho_{\uparrow\uparrow} & \rho_{\uparrow\downarrow} \\ \rho_{\downarrow\uparrow} & \rho_{\downarrow\downarrow} \end{pmatrix} \qquad\qquad |\rho\rangle\rangle = \begin{pmatrix} \rho_{\uparrow\uparrow} \\ \rho_{\uparrow\downarrow} \\ \rho_{\downarrow\uparrow} \\ \rho_{\downarrow\downarrow} \end{pmatrix}$$

(a) In Hilbert space   (b) In Liouville space

$$|\rho\rangle\rangle = \rho_{\uparrow\uparrow}|\uparrow\uparrow\rangle\rangle + \rho_{\uparrow\downarrow}|\uparrow\downarrow\rangle\rangle + \rho_{\downarrow\uparrow}|\downarrow\uparrow\rangle\rangle + \rho_{\downarrow\downarrow}|\downarrow\downarrow\rangle\rangle$$

(c) Density operator written as a linear
combination of eigenstates

Figure 2.2: Vectorization of the density operator for a spin-$\frac{1}{2}$ system

as $e^{(\mathcal{L}\Delta t)N}$ by slicing the time interval t into N equal intervals [14, 15]. Then, using Trotter splitting ($e^{\mathcal{L}\Delta t} \approx e^{\mathcal{L}_0 \Delta t} e^{\mathcal{L}_B \Delta t}$), we get

$$e^{\mathcal{L}t} = (e^{\Delta\mathcal{L}_0} e^{\Delta\mathcal{L}_B})^N, \tag{2.32}$$

where we have written $\mathcal{L}\Delta t$ simply as $\Delta\mathcal{L}$ for compactness.

Next we split the system path into N intervals of equal duration by inserting

resolutions of identity between each $e^{\Delta\mathcal{L}_0}e^{\Delta\mathcal{L}_B}$.

$$|\rho_t(t)\rangle\rangle = (e^{\Delta\mathcal{L}_0}e^{\Delta\mathcal{L}_B})^N|\rho(0)\rangle\rangle\,|\rho_B(0)\rangle\rangle$$

$$= e^{\Delta\mathcal{L}_0}e^{\Delta\mathcal{L}_B}\hat{\mathbb{1}}e^{\Delta\mathcal{L}_0}e^{\Delta\mathcal{L}_B}\hat{\mathbb{1}}\ldots\hat{\mathbb{1}}e^{\Delta\mathcal{L}_0}e^{\Delta\mathcal{L}_B}\hat{\mathbb{1}}|\rho(0)\rangle\rangle\,|\rho_B(0)\rangle\rangle$$

$$= \sum_{S_0,..,S_{N-1}}\sum_{B_0,..,B_{N-1}}e^{\Delta\mathcal{L}_0}e^{\Delta\mathcal{L}_B}|S_{N-1}\rangle\rangle\langle\langle S_{N-1}||B_{N-1}\rangle\rangle\langle\langle B_{N-1}|$$

$$\times\, e^{\Delta\mathcal{L}_0}e^{\Delta\mathcal{L}_B}\ldots|S_1\rangle\rangle\langle\langle S_1||B_1\rangle\rangle\langle\langle B_1|e^{\Delta\mathcal{L}_0}e^{\Delta\mathcal{L}_B}|S_0\rangle\rangle\langle\langle S_0|$$

$$\times\,|B_0\rangle\rangle\langle\langle B_0|\rho(0)\rangle\rangle\,\rho_B(0)\rangle\rangle$$

$$(2.33)$$

Since $\mathcal{L}_0$ is the free system Liouvillian, it acts only on the system states. Whereas, $\mathcal{L}_B$ contains the Liouvillian for bath as well as system-bath interaction. Hence, we can separate the system and bath terms.

$$|\rho_t(t)\rangle\rangle = \sum_{S_0,..,S_{N-1}}e^{\Delta\mathcal{L}_0}|S_{N-1}\rangle\rangle\langle\langle S_{N-1}|e^{\Delta\mathcal{L}_0}\ldots|S_1\rangle\rangle\langle\langle S_1|e^{\Delta\mathcal{L}_0}|S_0\rangle\rangle$$

$$\times\,\langle\langle S_0|\rho(0)\rangle\rangle\times\sum_{B_0,..,B_{N-1}}e^{\Delta\mathcal{L}_B}|B_{N-1}\rangle\rangle\langle\langle B_{N-1}|e^{\Delta\mathcal{L}_B}\ldots|B_1\rangle\rangle$$

$$\times\,\langle\langle B_1|e^{\Delta\mathcal{L}_B}|B_0\rangle\rangle\langle\langle B_0||\rho_B(0)\rangle\rangle\quad(2.34)$$

The reduced density operator is obtained by taking a trace over the bath degrees of freedom.

$$\rho(t) = \sum_{B_N}\langle\langle B_N|\rho_t(t)\rangle\rangle \qquad (2.35)$$

The matrix element of the reduced density operator at time t_N is

$$\langle\langle S_N|\rho(t)\rangle\rangle = \sum_{B_N}\langle\langle B_N|\langle\langle S_N|\rho_t(t)\rangle\rangle$$

$$= \sum_{S_0,..,S_{N-1}}\langle\langle S_N|e^{\Delta\mathcal{L}_0}|S_{N-1}\rangle\rangle\langle\langle S_{N-1}|e^{\Delta\mathcal{L}_0}\dots|S_1\rangle\rangle\langle\langle S_1|e^{\Delta\mathcal{L}_0}|S_0\rangle\rangle$$

$$\times\langle\langle S_0|\rho(0)\rangle\rangle \sum_{B_0,..,B_N}\langle\langle B_N|e^{\Delta\mathcal{L}_B}|B_{N-1}\rangle\rangle\langle\langle B_{N-1}|e^{\Delta\mathcal{L}_B}\dots|B_1\rangle\rangle$$

$$\times\langle\langle B_1 e^{\Delta\mathcal{L}_B}|B_0\rangle\rangle\langle\langle B_0|\rho_B(0)\rangle\rangle$$

$$= \sum_{S_0,..,S_{N-1}} F(\{S_k\})\, I(\{S_k\})\, \langle\langle S_0|\rho_s(0)\rangle\rangle.$$

$$(2.36)$$

The functional $F(\{S_k\})$ is the free part of the evolution and is given as

$$F(\{S_k\}) = \sum_{S_0,..,S_{N-1}}\prod_{j=1}^{N}\langle\langle S_j|e^{\Delta\mathcal{L}_0}|S_{j-1}\rangle\rangle. \qquad (2.37)$$

Whereas, the functional $I(\{S_k\})$ is the *discretized Feynman-Vernon influence functional*. It contains the complete information regarding the bath's influence on the evolution of the system. It reads

$$I(\{S_k\}) = \sum_{B_0,..,B_N}\prod_{j=1}^{N}\langle\langle B_j|e^{\Delta\mathcal{L}_B}|B_{j-1}\rangle\rangle\langle\langle B_0|\rho_B(0)\rangle\rangle \qquad (2.38)$$

We assume that the bath is initially in thermal equilibrium at temperature T, $\rho_B(0) = \frac{1}{\mathcal{Z}_B}\exp\left(-\frac{H_B}{T}\right)$, where $\mathcal{Z}$ is the partition function, and carry out the summations. This yields the following expression for the influence functional

$$I(\{S_k\}) = \exp\left(-\sum_{k=1}^{N}\sum_{k'=1}^{k}(s_k^+ - s_k^-)(\eta_{k-k'}\, s_{k'}^+ - \eta_{k-k'}^*\, s_{k'}^-)\right) \qquad (2.39)$$

The coefficients $\eta_{k-k'}$ that quantify the non-Markovian interaction between the reduced system at different times t_k and $t_{k'}$ are as given in Eq. (2.26)

The time evolved system density operator then attains the following form

$$\rho_{j_N}(t_N) = \sum_{j_1,\ldots,j_{N-1}} \left(\prod_{n=1}^{N}\prod_{k=0}^{n-1} \tilde{I}_k(j_n, j_{n-k})\right)\rho_{j_1} \tag{2.40}$$

$\rho_{j_k}(t_k)$ is the matrix element of the density operator at timestep k. Each index j runs from 1 to d^2.

Here we define the influence functions

$$\tilde{I}_k(S_l, S_{l'}) = \begin{cases} e^{-\phi(S_l, S_{l'})} & l - l' \neq 1 \\ \langle\langle S_1| e^{\Delta\mathcal{L}_0}|S_0\rangle\rangle e^{-\phi(S_l, S_{l'})} & l - l' = 1, \end{cases} \tag{2.41}$$

with

$$\phi(S_l, S_{l'}) = (s_l^+ - s_l^-)(\eta_{l-l'}\ s_{l'}^+ - \eta_{l-l'}^*\ s_{l'}^-) \tag{2.42}$$

2.3   ADT Scheme

Having derived the related mathematics, lets re-examine the time evolution of the non-Markovian system in detail. Moreover, we introduce the Augmented Density Tensor (ADT) scheme and the tensor network representation.
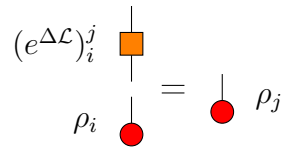

Figure 2.3: Pictorial representation of the evolution of the Markovian system

We begin with the evolution of the Markovian system which reads,

$$\rho_j(t + \Delta) = [e^{\Delta\mathcal{L}}]_i^j\ \rho_i(t). \tag{2.43}$$

In tensor network representation, a tensor is represented by an arbitrary geometrical shape having multiple protruding *legs*. The number of legs is

equal to the rank of the tensor and each leg has an n-dimensional local state space called the bond dimension. For example, for T_{ijk}, a tensor of rank 3, drawn as shown in Fig. 2.4. The bond dimensions of i, j and k are 5, 4 and 3 respectively. In this notation, the density operator $|\rho\rangle\rangle$ is represented by a circle with one leg whereas, the propagator $e^{\Delta\mathcal{L}}$ is shown by a square with two legs. The joining of legs in Fig. 2.3 represents tensor contraction as described by Eq. (2.43).

(a) A rank-3 tensor, T_{ijk}, of dimensions $(5, 4, 3)$
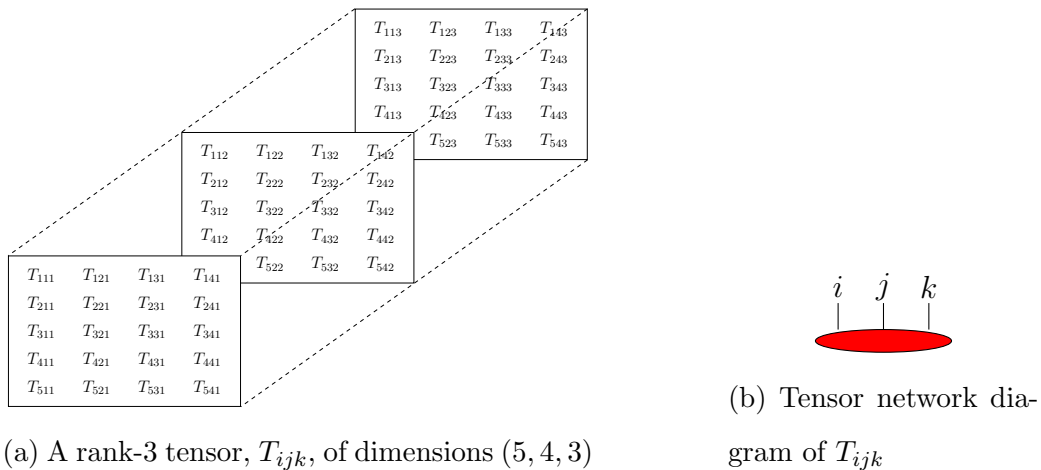
(b) Tensor network diagram of T_{ijk}

Figure 2.4: Tensor network representation

Unlike a Markovian system, the current state of a non-Markovian system is affected by the previous states of the system. Due to this, it is necessary to keep a record of the previous states. Lets see how this can be done for a two-level system.

At time t_1, the state of the reduced system is written as following

$$|\rho(t_1)\rangle\rangle = \begin{pmatrix} \rho_1(t_1) \\ \rho_2(t_1) \\ \rho_3(t_1) \\ \rho_4(t_1) \end{pmatrix} \tag{2.44}$$

16

To find the density operator at time t_2, we must consider all the possible paths the system can take to evolve from t_1 to t_2. The arrows in Fig. 2.5 show all the possible correlations between the elements of the density operators at the two times.
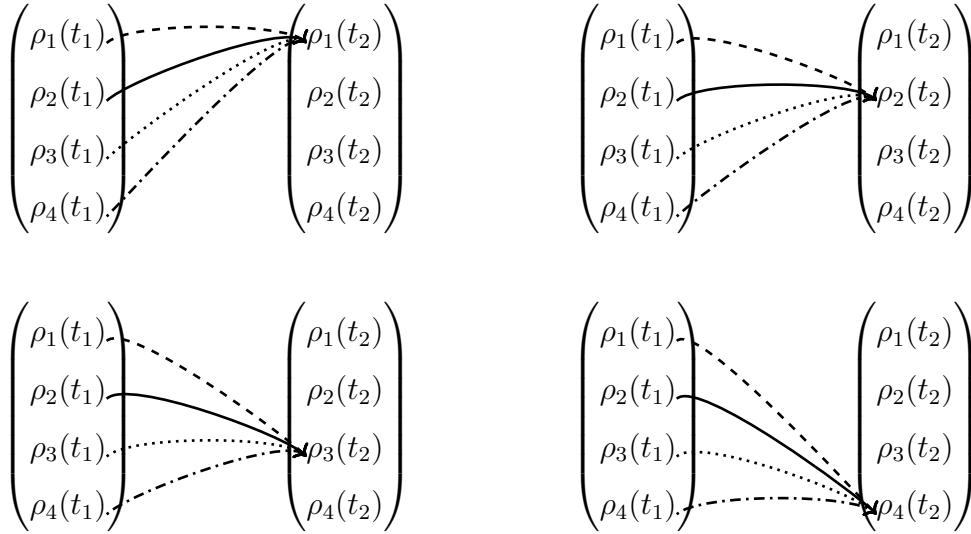

Figure 2.5: Correlations between the density operators at time t_1 and t_2

To record the probability amplitudes for all the possible trajectories, we will need a $d^2 \times d^2$ matrix. At the next step, we will need a tensor of rank 3 to store this information as shown in Fig. 2.6.

At each step, the size of the augmented density tensor (ADT) grows by one rank [15]. The ADT stores the set of amplitudes weighting each of the trajectories the reduced system could have taken through its Hilbert space in the previous timesteps of the evolution. The reduced system state after time t_N is given by the N-rank tensor, $A^{j_1,j_2,...,j_N}$. The ADT Scheme is based on quasi-adiabatic path integral (QUAPI) approach originally proposed by Makri and Makarov [16, 17].

17

(a) Density operator at t_1
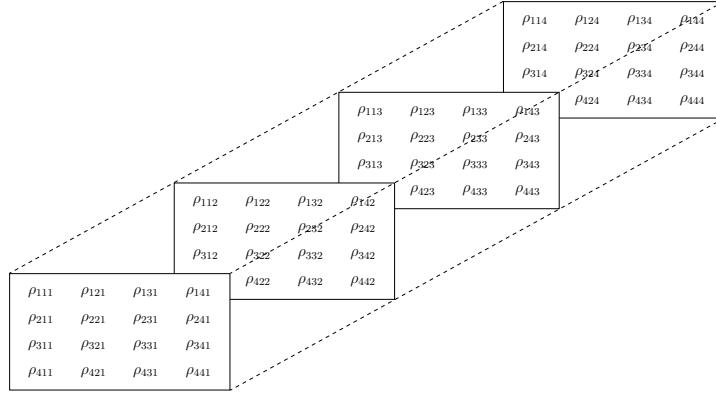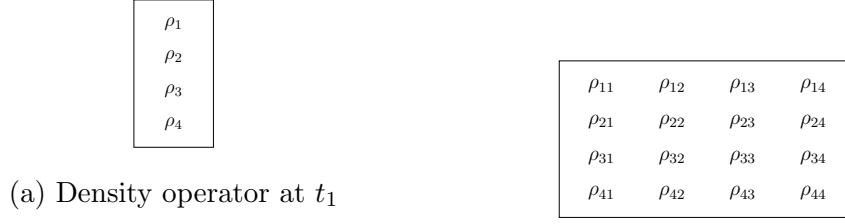

(b) ADT of rank-3 at t_3

Figure 2.6: Augmented Density Tensors

The products of the discretized influence functions in Eq. (2.40) give the components of the ADT. $\tilde{I}_k(j_n, j_{n-k})$ connects the evolution of the state j_n to the amplitude of the state j_{n-k}, k timesteps ago. For $N = 2$, Eq. (2.40) reads

$$\rho_{j_2} = \sum_{j_1} \left(\tilde{I}_0(j_1, j_1) \, \tilde{I}_0(j_2, j_2) \, \tilde{I}_1(j_2, j_1) \right) \rho_{j_1}. \tag{2.45}$$

For $N = 3$, it reads

$$\rho_{j_3} = \sum_{j_1, j_2} \left(\tilde{I}_0(j_1, j_1) \, \tilde{I}_0(j_2, j_2) \, \tilde{I}_1(j_2, j_1) \tilde{I}_0(j_3, j_3) \, \tilde{I}_1(j_3, j_2) \, \tilde{I}_2(j_3, j_1) \right) \rho_{j_1} \tag{2.46}$$

Fig. 2.7 shows a schematic representation of the action of the influence functions on the density vector.

18

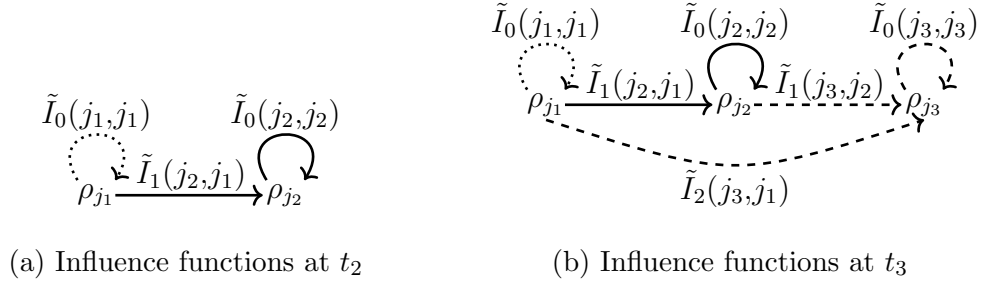(a) Influence functions at t_2 (b) Influence functions at t_3

Figure 2.7: Influence Functions

Next, we define our scheme in tensor network representation. The double product in Eq. (2.40) can be defined as a $(2n-1)$-index tensor,

$$B_{i_{n-1},...,i_1}^{j_N,j_{N-1},...,j_1}, \tag{2.47}$$

and the 1-index initial ADT is defined as

$$A^{j_1} = \tilde{I}_0(j_1, j_1)\rho_{j_1}(t_1). \tag{2.48}$$

The ADT is evolved iteratively by the successive contraction with the propagator tensor, B. The first contraction yields a 2-index ADT of the form shown in Fig. 2.10. It describes the full state and history at t_2.

$$A^{j_2,j_1} = B_{i_1}^{j_2,j_1} A^{i_1} \tag{2.49}$$

At the next step, the 3-index ADT is as shown in Fig. 2.10.

$$A^{j_3,j_2,j_1} = B_{i_2,i_1}^{j_3,j_2,j_1} A^{i_2,i_1} \tag{2.50}$$

The nth step reads

$$A^{j_n,j_{n-1},...,j_1} = B_{i_n,i_{n-1},...,i_1}^{j_n,j_{n-1},...,j_1} A^{i_n,i_{n-1},...,i_1} \tag{2.51}$$

The reduced density operator at time, t_n can then be found by performing summations over the ADT,

$$\rho_{j_n} = \sum_{j_{n-1},...,j_1} A^{j_n,j_{n-1},...,j_1} \tag{2.52}$$

19

At each timestep, the size of the ADT grows by one index in order to record the growing system history. To store the ADT we need to store d^2 numbers. If the ADT is allowed to grow indefinitely, the exponential storage requirements quickly cause memory problems. To encounter this problem, we assume that the bath has a finite memory. This is the *finite memory approximation*. This approximation is justified since for an infinite bosonic bath, the correlation function $C(t)$ decays to zero in finite time. This means that the influence functions $\tilde{I}$ have no effect once $t_k = k\Delta t$ exceeds the bath correlation time, τ_C. Therefore, we propagate the ADT containing only previous $K = \frac{\tau_C}{k\Delta t}$ timesteps.

In the *grow* phase, by successive application of asymmetric B tensors as described above, we allow the ADT to grow to a tensor of rank K, $A^{j_K, j_{K-1}, \ldots, j_1}$. The last step of the grow phase reads

$$A^{j_K, j_{K-1}, \ldots, j_1} = B^{j_K, j_{K-1}, \ldots, j_1}_{i_{K-1}, \ldots, i_1} A^{i_{K-1}, \ldots, i_1} \tag{2.53}$$

At the next timestep, we enter into the *propagate* phase. The correlations due to the oldest timestep are left out. The ADT is then evolved by the successive contraction with B tensors as shown in Fig. 2.11,

$$A^{j_{K+1}, j_K, \ldots, j_2}(t + \Delta t) = B^{j_{K+1}, j_K, \ldots, j_2}_{i_K, i_{K-1}, \ldots, i_1} A^{i_K, i_{K-1}, \ldots, i_1}(t) \tag{2.54}$$

$$A^{j_{K+2}, j_{K+1}, \ldots, j_3}(t + \Delta t) = B^{j_{K+2}, j_{K+1}, \ldots, j_3}_{i_{K+1}, i_K, \ldots, i_2} A^{i_{K+1}, i_K, \ldots, i_2}(t) \tag{2.55}$$

The nth step reads

$$A^{j_n, j_{n-1}, \ldots, j_{n-K+1}}(t + \Delta t) = B^{j_n, j_{n-1}, \ldots, j_{n-K+1}}_{i_{n-1}, i_{n-2}, \ldots, i_{n-K}} A^{i_{n-1}, i_{n-2}, \ldots, i_{n-K}}(t) \tag{2.56}$$

With the memory cutoff, the size of the ADT remains fixed. But it still needs d^{2K} numbers to be stored. For typical simulations, one can only go up to $K \sim 20$ before the storage capacity runs out. This is a limitation since one can only include the correlations present in the near-history and cannot keep the ones that go a little far back in time.

2.4 Matrix Product States and Matrix Product Operators

An efficient way to store and evaluate high-rank tensors is to decompose them into products of low-rank tensors [18, 19]. The ADT is decomposed into Matrix Product States (MPSs) and the propagator tensors B are decomposed into Matrix Product Operators (MPOs). Using MPS/MPO representation, we can grow and propagate the ADT up to $K \sim 10^2$ [8]. This is an order of magnitude improvement from the ADT scheme [15].

The ADT is decomposed by successively performing Singlar Value Decompositions (SVDs) and truncating the singular values [20]. Here, we illustrate the method in detail. As a first step, we reshape the rank-K ADT, $A^{j_1, j_2, \ldots, j_K}$ with $D^K = d^{2K}$ elements into a matrix Ψ of dimensions $(D \times D^{K-1})$,

$$A^{j_1, j_2, \ldots, j_K} \equiv \Psi_{j_1, j_2 j_3 \ldots j_K} \tag{2.57}$$

An SVD of Ψ gives

$$\Psi_{j_1, j_2 j_3 \ldots j_K} = U_{j_1, \alpha_1} S_{\alpha_1, \alpha_1} V^\dagger_{\alpha_1, (j_2 j_3 \ldots j_K)} \tag{2.58}$$

Here, U and V are unitary matrices and S is a diagonal matrix whose non-zero entries are the singular values of the matrix Ψ. Next, we discard the singular values λ_α smaller than some cutoff λ_c and also discard the corresponding columns and rows of U and V matrices respectively, thereby reducing their sizes. The truncated S and V matrices are then multiplied to obtain the matrix $\Psi_{\alpha_1, j_2 j_3 \ldots j_K}$ and the U matrix is written as $a^{j_1}_{\alpha_1}$.

$$A^{j_1, j_2, \ldots, j_K} = \Psi_{j_1, j_2 j_3 \ldots j_K} = \sum_{\alpha_1}^{r_1} a^{j_1}_{\alpha_1} \Psi_{\alpha_1, j_2 j_3 \ldots j_K} \tag{2.59}$$

where r_1 is the number of singular values after truncation. It is the bond dimension. α_1 runs from 1 to r_1 ($r_1 < D$). Again, we reshape the $\Psi_{\alpha_1, j_2 j_3 \ldots j_K}$

21

into a new matrix $\Psi_{\alpha_1 j_2, j_3 \ldots j_K}$ An SVD is performed and the singular values are truncated. This gives us

$$\Psi_{(\alpha_1 j_2),(j_3 j_4)} = U_{(\alpha_1 j_2),\alpha_2} \; S_{\alpha_2,\alpha_2} \; V^\dagger_{\alpha_2,(j_3 j_4)} \approx \sum_{\alpha_1,\alpha_2}^{r_1,r_2} a^{j_2}_{\alpha_1,\alpha_2} \; \Psi_{\alpha_2,(j_3 j_4)} \qquad (2.60)$$

This procedure is repeated iteratively to finally obtain the ADT in the form of a Matrix Product State.

$$A_{j_1,j_2,\ldots j_K} = \sum_{\alpha_1,\ldots,\alpha_{K-1}} a^{j_1}_{\alpha_1} \; a^{j_2}_{\alpha_1,\alpha_2} \; a^{j_3}_{\alpha_2,\alpha_3} \; \ldots a^{j_{K-1}}_{\alpha_{K-2},\alpha_{K-1}} a^{j_K}_{\alpha_{K-1}} \qquad (2.61)$$

Since we started the decomposition from the left, we obtained products of left-normalized matrices. An MPS that contains only the left-normalized matrices is called a left-canonical MPS.
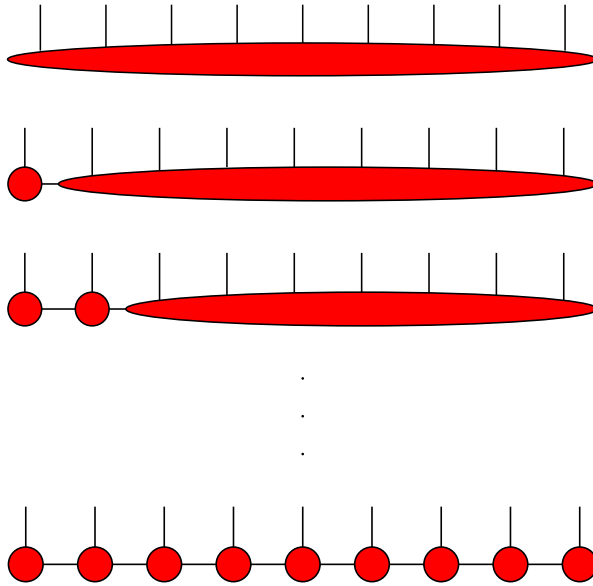

Figure 2.8: Graphical representation of an iterative decomposition of a rank-K ADT into MPS, starting from the left, for $K = 9$

This decomposition is represented graphically as shown in Fig. 2.8. The ADT is represented by an ellipse. The physical indices j_1 through j_K stick out
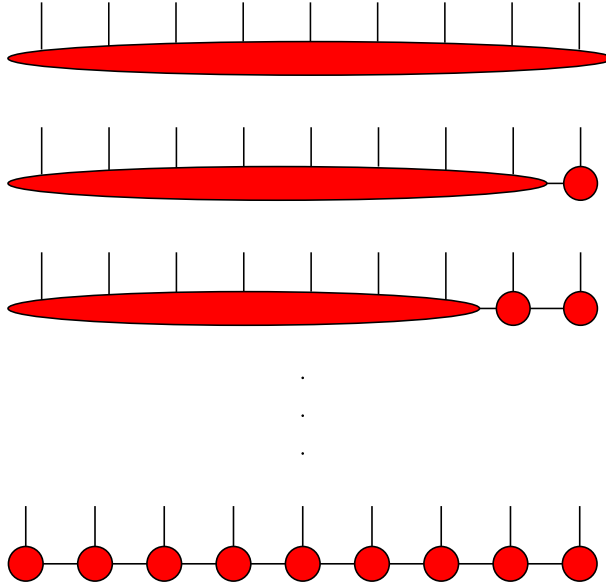
Figure 2.9: Graphical representation of an iterative decomposition of an rank-K ADT into MPS, starting from the right, for $K = 9$

of the ellipse vertically. After the first decomposition we have a circle on the left representing $a^{j_1}_{\alpha_1}$ and an ellipse on the right representing $A^{\alpha_1, j_2, \ldots, j_K}$. The horizontal line represents the auxiliary bond, α_1. As a rule, the connected lines between adjacent matrices, called *bonds*, are always summed over. The process of separating out a circle is repeated in the next step and thereafter to obtain a train of circles representing the MPS.

Similarly, we can start decomposing from the right to obtain a right-canonical MPS. This is shown in Fig. 2.9.

The propagator tensors B are decomposed into Matrix Product Operators in a similar way [21]. The TEMPO algorithm is implemented by successive contractions of MPSs and MPOs [20, 22]. The application of an MPO on an MPS results in an ADT which is then decomposed into an MPS again using SVDs and truncation. To find the most efficient MPS representation of ADT, it is important to sweep from both left to right and then right to
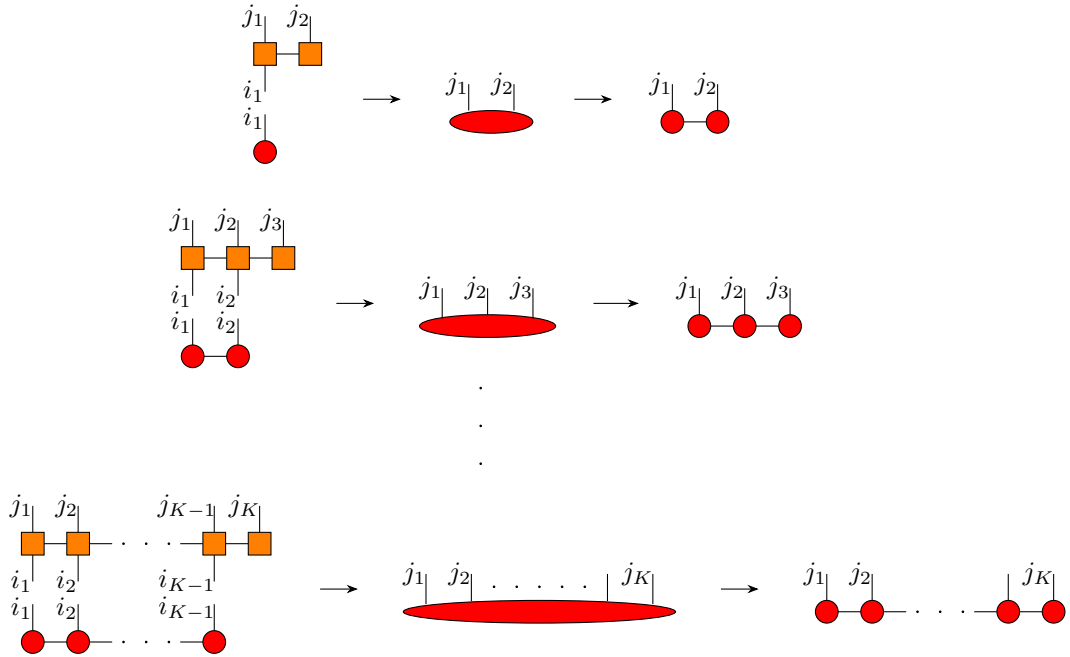
Figure 2.10: Grow phase

left as described above [23]. The grow phase as outlined in (2.49) through (2.51) is illustrated in Fig. 2.10. The propagate phase as outlined in (2.54) through (2.56) is illustrated in Fig. 2.11. In Fig. 2.11, the semi-circle represents a vector whose elements are all equal to 1. The MPS of the oldest timestep is contracted with this vector in order to realize the finite memory approximation. In this way, we can study the time evolution of non-Markovian systems upto very large values of K.

Figure 2.11: Propagate phase

Chapter 3

Results

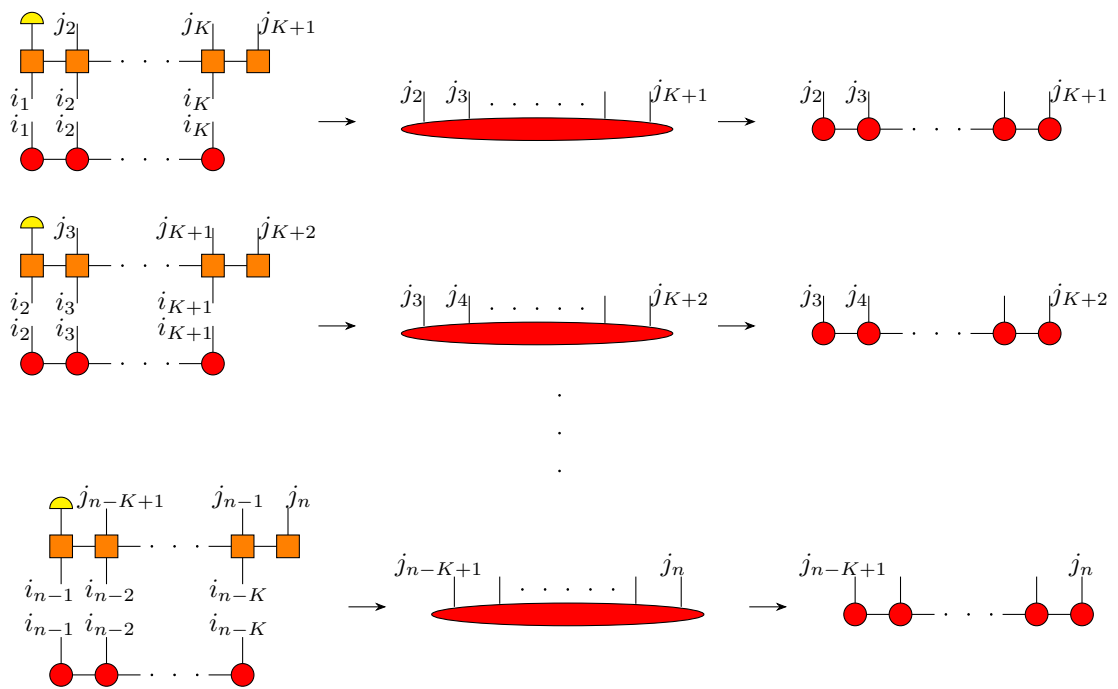In this chapter, the method developed in the previous chapter is applied to study the dynamics of a quantum dot (QD) coupled to a cavity. The method was primarily developed to study the non-Markovian dynamics of open quantum systems. It has been applied to demonstrate the phase transitions in the Spin-Boson Model, which has long been the testing ground for open quantum systems, and the environment mediated interactions in the model of two spins in a common environment, for which the non-Markovian dynamics are not accessible using the existing methods [8].

Here, we demonstrate the flexibility of TEMPO by applying it to a more complicated example, that of a two-level system coupled to both a single harmonic oscillator and a bath. As a prototype for such a system, we consider a quantum dot with exciton-phonon interactions placed in a cavity [24, 7]. We use TEMPO to model the phonon bath but treat the cavity mode as part of the reduced system. We show the phonon-induced damping of Rabi oscillations in higher excitation spaces. Our work demonstrates the utility of TEMPO in easily handling a model with a relatively large Hilbert space of the reduced system. We will start by demonstrating the damping

of Rabi oscillations in a single excitation space and its relation with the different coupling strengths and temperature. Then, we will go on to apply the method in higher excitation spaces and see whether the same effect can also be observed there.

A quantum dot is a nanometer-sized region of a semiconductor material on which a thin layer of another semiconductor material is deposited, e.g. in InGaAs quantum dots, GaAs substrate is coated with a thin layer of InAs. Due to the difference in lattice constants, the layer of InAs experiences a strain and begins to form 'dome-shaped' islands [25, 4]. This also leads to creation of a band-gap which confines the charge carriers in the dot in all three dimensions. The resulting electronic and optical properties of the quantum dot are quite similar to that of an atom. For this reason, they are often referred to as 'artificial atoms'.

Quantum dots are a hot topic of research nowadays due to their applications in a plethora of emerging quantum technologies [26, 27]. By manufacturing quantum dots of different sizes, the energy difference in quantized levels can be controlled to obtain the emission of light of desired frequencies. From Light-Emitting Diodes (LEDs), solar cells [28] and phototransistors [29] to their uses in biosensing and biomedicine, these efficient semiconductor nanocrystals are proving to be of immense industrial value. They are also a strong candidate for their use in quantum hardware as single photon sources [30, 31, 32].

Besides these industrial applications, a single quantum dot also serves well as a typical open quantum system. The phononic degrees of freedom act as an environment to the excitonic levels. This makes it an ideal system to apply and test new methods developed for open quantum systems.

Many interesting phenomena result due to phonon bath coupling with cavity-

QD system. One of these phenomena namely the phonon-induced damping of Rabi oscillations is demonstrated here [33, 34]. The model considered here consists of a two-level system, ground state and a single excitonic state, with an energy splitting ϵ_0 coupled to both a single cavity mode and a phonon bath. The two-level system is represented using the Pauli spin operators. The phonon bath is assumed to be a harmonic bath i.e. it is assumed to be composed of an infinite number of harmonic oscillators. The two-level system and the cavity mode are treated as the reduced system. We use the number conserving Jaynes-Cummings Hamiltonian to model the dot-cavity interaction, and TEMPO to model the phonon bath.

The Jaynes-Cummings Hamiltonian for dot-cavity is then given by

$$H_0 = \epsilon_0 \sigma_n + g \left(\hat{a}^\dagger \sigma^+ + \hat{a} \sigma^- \right) + \omega_{cav} \hat{a}^\dagger \hat{a} \tag{3.1}$$

where ω_{cav} is the frequency of the cavity mode. The operator σ_n gives the occupation number of the excitonic state. The ladder operators (σ^+ and σ^-) drive the transitions between the ground and the excited state of the two-level system. The creation and annihilation operators ($\hat{a}$ and $\hat{a}^\dagger$) create and annihilate a single photon in the cavity mode, respectively.

The behaviour of the phonon bath is characterized by the superohmic spectral density with Gaussian decay,

$$J(\omega) = \alpha \omega^3 \exp \left(- \left(\frac{\omega}{2\omega_c} \right)^2 \right) \tag{3.2}$$

where the α is the coupling strength and the cutoff frequency, ω_c depends on the spatial dimensions of the quantum dot. The bath coupling operator is taken to be the Pauli Spin Operator, σ_z.

When the excited and ground states of the quantum dot are defined as follows

$$|e\rangle = \begin{pmatrix} 1 \\ 0 \end{pmatrix} \quad and \quad |g\rangle = \begin{pmatrix} 0 \\ 1 \end{pmatrix},$$

the operator that gives the population of the excited state of the quantum dot is defined as

$$\sigma_n = \begin{pmatrix} 1 & 0 \\ 0 & 0 \end{pmatrix}.$$

Consider the simplest case in our model where there is only one excitation in the reduced system. Initially, the cavity is taken to be in ground state whereas the quantum dot is in excited state. The effective combined Hilbert space of the reduced system is then defined by the given states:

$$|0, e\rangle \quad and \quad |1, g\rangle$$

In the absence of a phonon bath i.e. $\alpha = 0$, we observe undamped Rabi oscillations as expected. The population of the cavity is inverted into that of the quantum dot. However, as α is increased, the phonon effects start taking over. The interaction with the phonon bath dampens the Rabi oscillations. For larger coupling strengths, the damping is stronger and the oscillations die out quickly. This can be seen in Fig. 3.1. Another interesting thing to note is, for larger coupling strengths, we see that the repeated measurements of the operator σ_n leads to the population getting shifted to the excited state of the quantum dot. This is the Quantum Zeno Effect. The Quantum Zeno Effect is a feature of the quantum-mechanical systems allowing a particle's evolution to be arrested by measuring it frequently enough with respect to some chosen measurement setting.

Furthermore, it can be observed that there is an increase in the decay rate of the oscillations with a rise in temperature. As the temperature is increased,
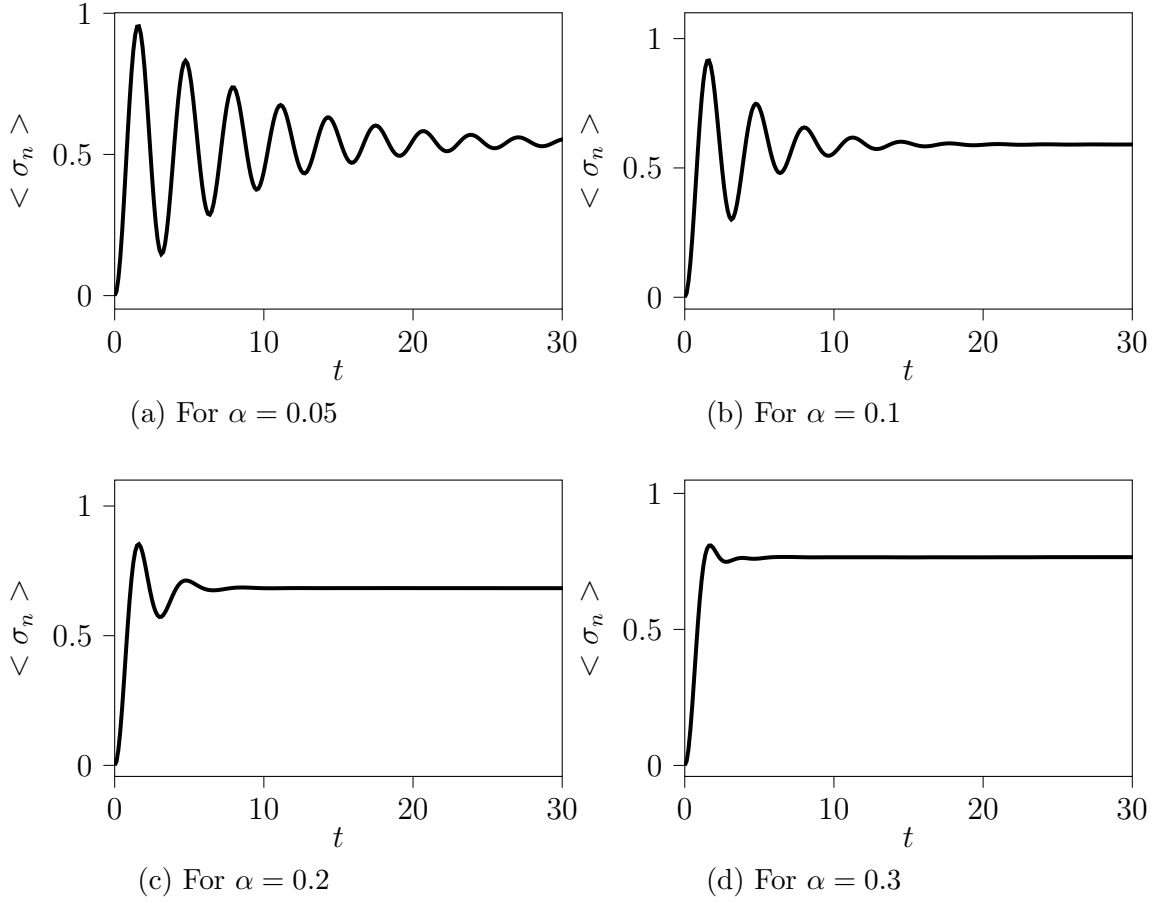
(a) For $\alpha = 0.05$

(b) For $\alpha = 0.1$

(c) For $\alpha = 0.2$

(d) For $\alpha = 0.3$

Figure 3.1: QD exciton occupation, $\langle \sigma_n \rangle$, for different coupling strengths, α

the oscillators in the phonon bath have increased vibrational energy. The damping effect of the phonon bath becomes stronger and the Rabi oscillations decay more rapidly. This increase in the decay rate of Rabi oscillations with increase in temperature can be seen in Fig. 3.2. The damping of these oscillations is a general phenomenon. It can be observed for all temperatures and coupling strengths. These results were obtained by propagating the system for 300 timesteps without any memory cutoff.

To further prove the robustness of the method, consider a more complicated problem that explores the higher excitation spaces of the reduced system.
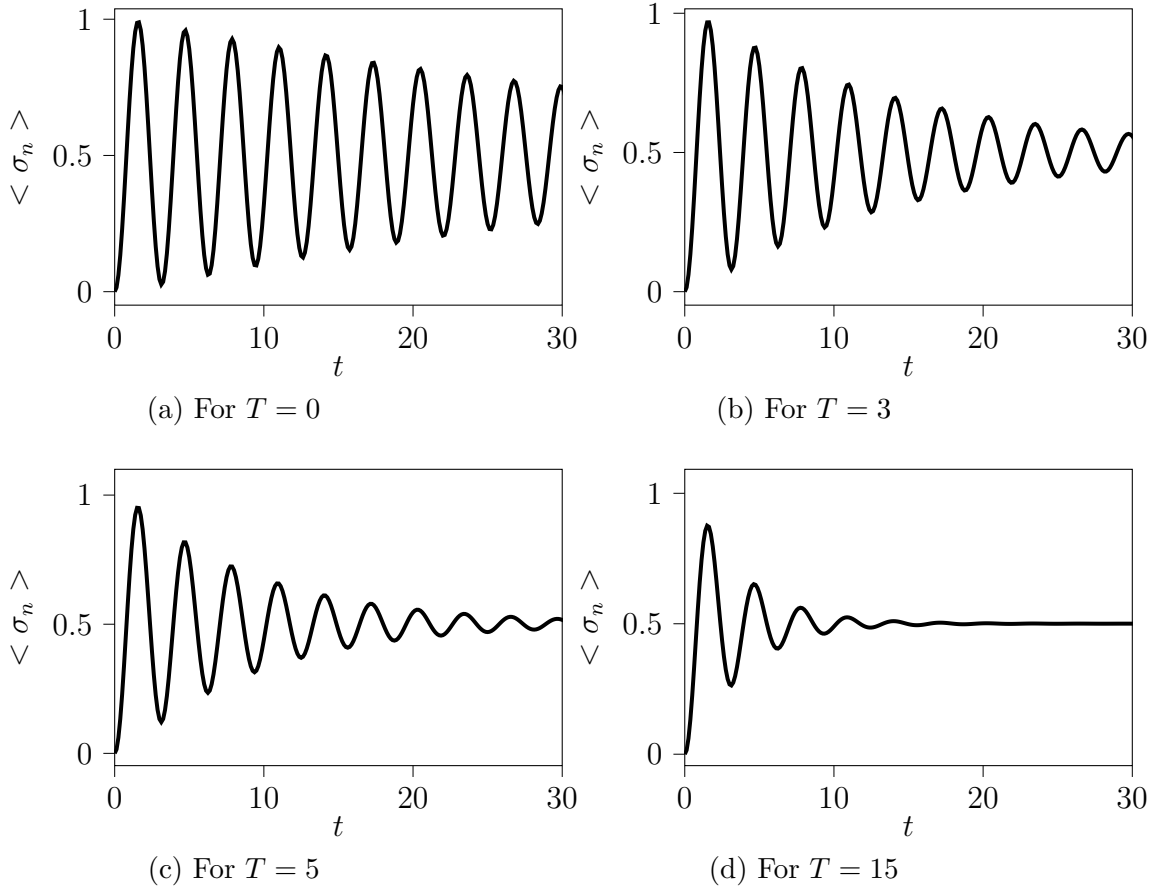
(a) For $T = 0$

(b) For $T = 3$

(c) For $T = 5$

(d) For $T = 15$

Figure 3.2: QD exciton occupation, $\langle \sigma_n \rangle$, for coupling strength, $\alpha = 0.01$ at different temperatures, T

The maximum number of allowed excitations in cavity is 3. Initially, the quantum dot is in excited state and the cavity is in a superposition state, $|\psi_{cav}\rangle = \frac{1}{\sqrt{3}} |1\rangle + \frac{1}{\sqrt{3}} |2\rangle + \frac{1}{\sqrt{3}} |3\rangle$. The Hilbert space of the reduced system

then, constitutes of the following states:

$$N_{ex} = 0 \ : \quad |0, g\rangle$$

$$N_{ex} = 1 \ : \quad |0, e\rangle \quad and \quad |1, g\rangle$$

$$N_{ex} = 2 \ : \quad |1, e\rangle \quad and \quad |2, g\rangle$$

$$N_{ex} = 3 \ : \quad |2, e\rangle \quad and \quad |3, g\rangle$$

$$N_{ex} = 4 \ : \quad |3, e\rangle$$

To observe the populations in these excitation spaces, we define the population operators as follows.

For $N_{ex} = 1$,

$$\sigma_{n_1} = |0, e\rangle \langle 0, e|$$

$$= |0\rangle \langle 0| \otimes |e\rangle \langle e|$$

$$= \begin{pmatrix} 1 & 0 & 0 & 0 \\ 0 & 0 & 0 & 0 \\ 0 & 0 & 0 & 0 \\ 0 & 0 & 0 & 0 \end{pmatrix} \otimes \begin{pmatrix} 1 & 0 \\ 0 & 0 \end{pmatrix}$$

Similarly, for higher excitation spaces, these operators are given as

$$\sigma_{n_2} = |1, e\rangle \langle 1, e| \qquad \sigma_{n_3} = |1, e\rangle \langle 1, e| \qquad \sigma_{n_4} = |3, e\rangle \langle 3, e|$$

Fig. 3.3 shows the population of excited state of quantum dot in all excitation spaces for $\alpha = 0.1$. For $N_{ex} = 0$ and $N_{ex} = 1$, the populations are zero throughout as they were zero initially. The line for $N_{ex} = 0$ has been omitted from Fig. 3.3 for clarity. For $N_{ex} = 2$, the oscillations occur between $|1, e\rangle \longleftrightarrow |2, g\rangle$, and for $N_{ex} = 3$, they occur between $|2, e\rangle \longleftrightarrow |3, g\rangle$. Independent damped Rabi oscillations are observed in each excitation space.
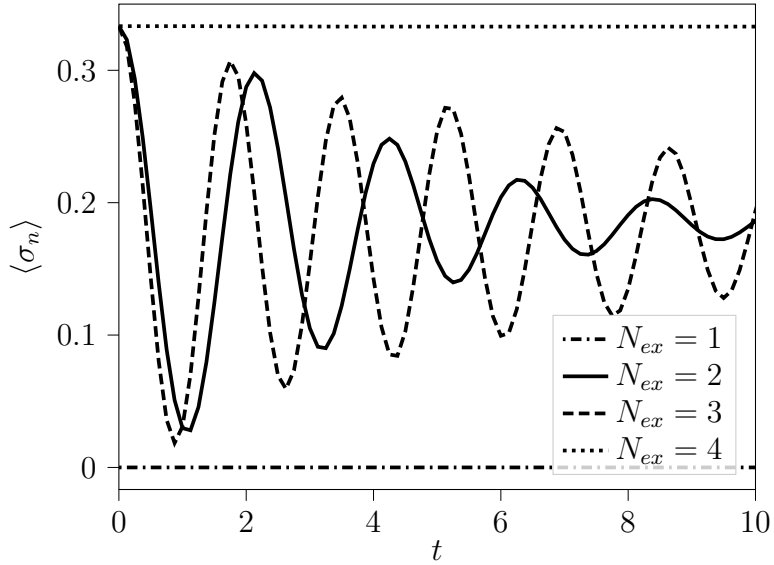
Figure 3.3: QD exciton occupation in all excitation spaces for $\alpha = 0.1$

For $N_{ex} = 4$, no oscillations are observed because the higher states for cavity such as $|4, g\rangle$ are not accessible.

In Fig. 3.4, the increased damping of oscillations due to stronger coupling with bath can be seen independently in the $N_{ex} = 3$ excitation space. Furthermore, the Quantum Zeno Effect is very prominent for larger coupling strengths i.e. $\alpha = 0.7$ and $\alpha = 1.5$.

The system was propagated for 100 timesteps. Again, these calculations were performed without a memory cutoff.
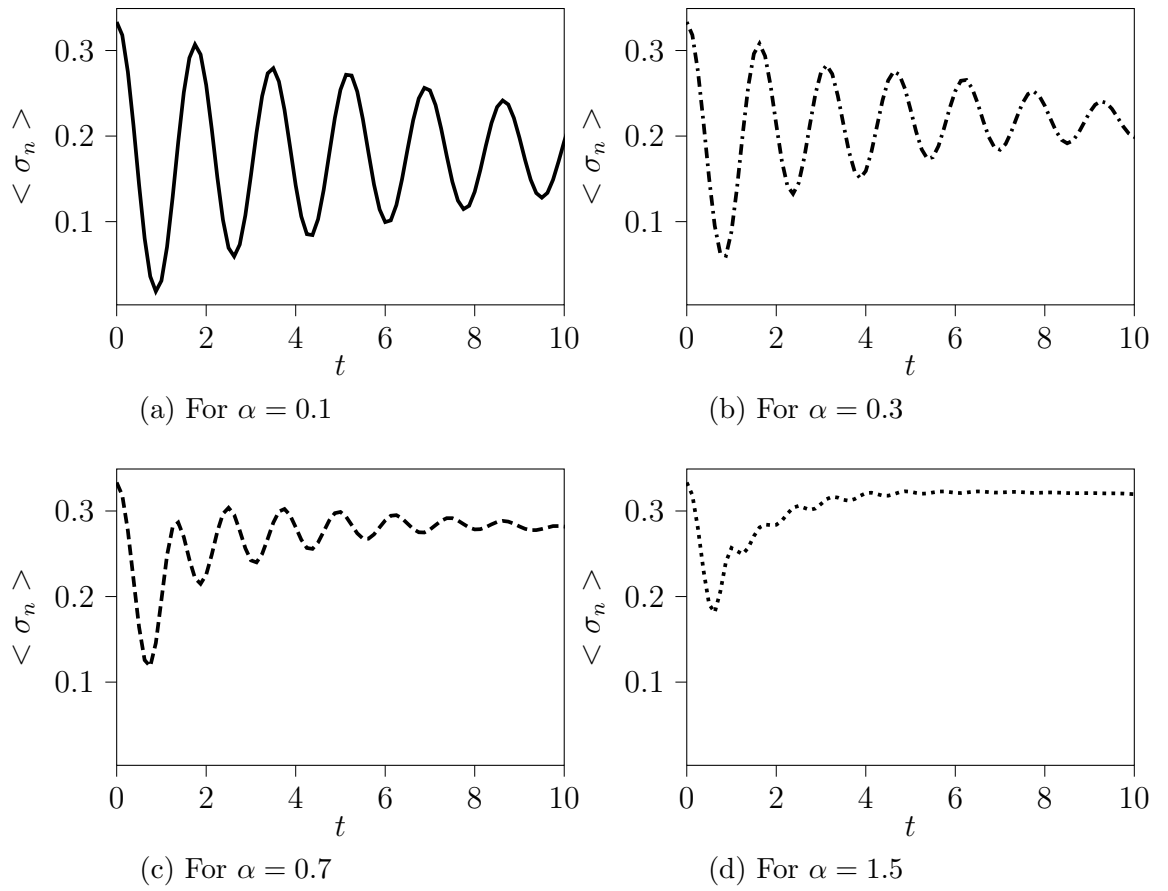
(a) For $\alpha = 0.1$

(b) For $\alpha = 0.3$

(c) For $\alpha = 0.7$

(d) For $\alpha = 1.5$

Figure 3.4: QD exciton occupation, $\langle \sigma_{n_3} \rangle$, in $N_{ex} = 3$ for different coupling strengths, α

Chapter 4

Conclusion

The rapid advancements in computer hardware have brought us to the brink of a new technological revolution, the Quantum Computing era. However, the realization of such a revolution needs a sound understanding of how quantum systems interact with their environments, and how to control them to retain coherence for long times. The technological advancements have also allowed us to probe and control these systems with increasing precision. The study of open quantum systems (OQSs) has, thus, become far important than ever. The methods for solving Markovian OQSs are extensively studied and well-developed. The general physical principles of the non-Markovian OQSs, however, are not well-established and the methods developed so far, to solve the dynamics of these systems are limited to certain parameter regimes.

An efficient method to study the non-Markovian dynamics, called Time-Evolving Matrix Product Operators (TEMPO), has been developed by Strathearn et. al. [8]. The method uses ADT to store the system's history, and uses Feynman Vernon Influence Functional to model bath. It can be used to solve for the dynamics of OQSs up to very large memory times. The key to the efficiency of the method is the use of Matrix Product States (MPSs) and

Matrix Product Operators (MPOs), which are a natural tool to represent very large tensor networks.

Our work demonstrates how TEMPO can solve for the dynamics of an OQS retaining the correlations for a long period of time. It also shows the way TEMPO can easily deal with a relatively large reduced system (8 states) without needing a memory cutoff. This is impossible to do using standard QUAPI techniques [16]. The robustness and efficiency of TEMPO is a huge improvement over the existing methods. This makes it an ideal technique to be used for more complicated problems in the theory of open quantum systems.

Despite being the best method available to solve non-Markovian dynamics, there are still some areas which can be improved. The method works relatively slowly for higher excitation spaces as the density matrix is larger, and larger ADT is propagated. It is also observed that the execution takes more time for larger values of coupling strengths because the correlations are stronger. As a result, the ADT is densely populated, so SVD and truncation are not as effective as they are for weak coupling regimes. SVD and truncation can be optimized by finding better ways to implement SVD and introduce an optimum cutoff for singular values.

The method involves solving a lot of integrals which are time-consuming. A double integral in η function as given in Eq. (2.26) is calculated at each timestep. The current implementation uses *scipy.integrate.quad* to compute these integrals. A huge improvement in this regard can be achieved by using *pathos.multiprocessing.Pool* to compute the integrals in parallel. Moreover, the current implementation TEMPO is in Python language, which is an interpreter language. The overall code can be made more efficient by implementing it in a compiler language such as C++ or Fortran.

In our work, we have examined a relatively simple phenomenon in quantum dots in order to focus on the details of the development and the working of the TEMPO method. However, the method is very powerful and the subject of exciton-phonon coupling is a rich and interesting one. More interesting phenomena such as the resonance fluorescence spectrum of a quantum dot can be studied using TEMPO. This will be the subject of future work.

Appendix A

Path integral formalism

Here we briefly introduce the path integral formalism for the evolution of a pure state, ψ and then, for the more general, density matrix, ρ.

For a time-independent Hamiltonian H, the time evolution of the wavefunction is given by

$$|\psi(t)\rangle = e^{-iHt} |\psi(0)\rangle . \tag{A.1}$$

Inserting a resolution of identity, we can write the above expression in coordinate representation as follows

$$\langle x_f|\psi(t)\rangle = \int dx_i \, \langle x_f| \, e^{-iHt} \, |x_i\rangle \, \langle x_i|\psi(0)\rangle . \tag{A.2}$$

The complex amplitude, $\langle x_f| \, e^{-iHt} \, |x_i\rangle$ is known as *propagator*, $\mathbf{K}(x_f, t|x_i, 0)$. It is the probability amplitude for the particle to go from point x_i to point x_f in time t. The path integral representation of the propagator is

$$\mathbf{K}(x_f, t; x_i, 0) = \int \mathcal{D}[x(t)] e^{iS[x(t)]}, \tag{A.3}$$

where $\mathcal{D}[x(t)]$ denotes integration over all possible paths with endpoints $x(0) = x_i$ and $x(t) = x_f$. The *phase factor* S is the classical action, $S = \int_0^t L(\dot{x}(t), x(t))dt$ where L is the *Lagrangian* of the classical particle.

Now we proceed to find the time evolution of the density matrix. In Heisenberg picture, we have

$$\rho(t) = e^{-iHt}\rho(0)e^{iHt} \qquad (A.4)$$

The matrix element of the time-evolved density matrix is

$$\langle x_f| \rho(t) |x_f'\rangle = \langle x_f| e^{-iHt}\rho(0)e^{iHt} |x_f'\rangle \qquad (A.5)$$

Inserting resolution of identities twice, we get

$$\langle x_f| \rho(t) |x_f'\rangle = \int dx_i dx_i' \langle x_f| e^{-iHt} |x_i\rangle \langle x_i| \rho(0) |x_i'\rangle \langle x_i'| e^{iHt} |x_f'\rangle \qquad (A.6)$$

$$\langle x_f| \rho(t) |x_f'\rangle = \int dx_i dx_i' \mathbf{J}(x_f, x_f', t; x_i, x_i', 0)\rho(x_i, x_i', 0) \qquad (A.7)$$

where $\mathbf{J}(x_f, x_f', t; x_i, x_i', 0) = \langle x_f| e^{-iHt} |x_i\rangle \langle x_i'| e^{iHt} |x_f'\rangle$ is the propagator for the density matrix. Its path integral representation is given by

$$\mathbf{J}(t; 0) = \int_a^b \mathcal{D}[x] \exp\left(iS[x]\right) \int_a^b \mathcal{D}[x'] \exp\left(-iS[x']\right) \qquad (A.8)$$

$$= \int_a^b \mathcal{D}[x]\mathcal{D}[x'] \exp\left(iS[x] - iS[x']\right). \qquad (A.9)$$

For clarity, we have omitted x coordinates in the argument of $\mathbf{J}$.

Bibliography

[1] R. E. Blankenship, D. M. Tiede, J. Barber, G. W. Brudvig, G. Fleming, M. Ghirardi, M. R. Gunner, W. Junge, D. M. Kramer, A. Melis, T. A. Moore, C. C. Moser, D. G. Nocera, A. J. Nozik, D. R. Ort, W. W. Parson, R. C. Prince, and R. T. Sayre, "Comparing Photosynthetic and Photovoltaic Efficiencies and Recognizing the Potential for Improvement," *Science*, vol. 332, pp. 805–809, May 2011.

[2] N. Lambert, Y.-N. Chen, Y.-C. Cheng, C.-M. Li, G.-Y. Chen, and F. Nori, "Quantum biology," *Nature Physics*, vol. 9, pp. 10–18, Jan. 2013. Number: 1 Publisher: Nature Publishing Group.

[3] U. Weiss, *Quantum Dissipative Systems*. WORLD SCIENTIFIC, 3 ed., Mar. 2008.

[4] Y. Masumoto, T. Takagahara, P. Avouris, K. von Klitzing, H. Sakaki, and R. Wiesendanger, eds., *Semiconductor Quantum Dots*. NanoScience and Technology, Berlin, Heidelberg: Springer, 2002.

[5] H.-P. Breuer and F. Petruccione, *The theory of open quantum systems*. Oxford ; New York: Oxford University Press, 2002.

[6] I. de Vega and D. Alonso, "Dynamics of non-Markovian open quantum systems," Feb. 2017.

[7] A. Strathearn, *Modelling Non-Markovian Quantum Systems Using Tensor Networks*. Springer Theses, Cham: Springer International Publishing, 2020.

[8] A. Strathearn, P. Kirton, D. Kilda, J. Keeling, and B. W. Lovett, "Efficient non-Markovian quantum dynamics using time-evolving matrix product operators," *Nature Communications*, vol. 9, p. 3322, Dec. 2018.

[9] R. P. Feynman, "Space-Time Approach to Non-Relativistic Quantum Mechanics," *Reviews of Modern Physics*, vol. 20, pp. 367–387, Apr. 1948. Publisher: American Physical Society.

[10] L. Bovard, W. Heisenberg, M. Born, and P. Jordan, "An Introduction to the Path Integral Approach to Quantum Mechanics," p. 3.

[11] M. Patriarca, "Statistical correlations in the oscillator model of quantum dissipative systems," *Il Nuovo Cimento B Series 11*, vol. 111, pp. 61–72, Jan. 1996.

[12] M. Carrega, P. Solinas, A. Braggio, M. Sassetti, and U. Weiss, "Functional Integral approach to time-dependent heat exchange in open quantum systems: general method and applications," *New Journal of Physics*, vol. 17, p. 045030, Apr. 2015.

[13] M. Kilgour, B. K. Agarwalla, and D. Segal, "Path-integral methodology and simulations of quantum thermal transport: Full counting statistics approach," *The Journal of Chemical Physics*, vol. 150, p. 084111, Feb. 2019.

[14] N. S. Dattani, F. A. Pollock, and D. M. Wilkins, "Analytic influence functionals for numerical Feynman integrals in most open quantum systems," Mar. 2012.

[15] A. Strathearn, B. W. Lovett, and P. Kirton, "Efficient Real-Time Path Integrals for Non-Markovian Spin-Boson Models," *New Journal of Physics*, vol. 19, p. 093009, Sept. 2017.

[16] N. Makri and D. E. Makarov, "Tensor propagator for iterative quantum time evolution of reduced density matrices. I. Theory," *The Journal of Chemical Physics*, vol. 102, pp. 4600–4610, Mar. 1995. Publisher: American Institute of Physics.

[17] N. Makri and D. E. Makarov, "Tensor propagator for iterative quantum time evolution of reduced density matrices. II. Numerical methodology," *The Journal of Chemical Physics*, vol. 102, pp. 4611–4618, Mar. 1995. Publisher: American Institute of Physics.

[18] R. Orus, "A Practical Introduction to Tensor Networks: Matrix Product States and Projected Entangled Pair States," *Annals of Physics*, vol. 349, pp. 117–158, Oct. 2014.

[19] J. C. Bridgeman and C. T. Chubb, "Hand-waving and interpretive dance: an introductory course on tensor networks," *Journal of Physics A: Mathematical and Theoretical*, vol. 50, p. 223001, June 2017.

[20] U. Schollwoeck, "The density-matrix renormalization group in the age of matrix product states," *Annals of Physics*, vol. 326, pp. 96–192, Jan. 2011.

[21] C. Hubig, I. P. McCulloch, and U. Schollwöck, "Generic construction of efficient matrix product operators," *Physical Review B*, vol. 95, p. 035129, Jan. 2017.

[22] R. N. C. Pfeifer, G. Evenbly, S. Singh, and G. Vidal, "NCON: A tensor network contractor for MATLAB," Aug. 2015.

[23] S. Paeckel, T. Köhler, A. Swoboda, S. R. Manmana, U. Schollwöck, and C. Hubig, "Time-evolution methods for matrix-product states," *Annals of Physics*, vol. 411, p. 167998, Dec. 2019.

[24] N. Ishida, T. Byrnes, F. Nori, and Y. Yamamoto, "Photoluminescence of a microcavity quantum dot system in the quantum strong-coupling regime," *Scientific Reports*, vol. 3, p. 1180, Dec. 2013.

[25] A. Nazir and D. P. S. McCutcheon, "Modelling exciton-phonon interactions in optically driven quantum dots," *Journal of Physics: Condensed Matter*, vol. 28, p. 103002, Mar. 2016.

[26] M. A. Cotta, "Quantum Dots and Their Applications: What Lies Ahead?," *ACS Applied Nano Materials*, vol. 3, pp. 4920–4924, June 2020.

[27] S. Kubendhiran, Z. Bao, K. Dave, and R.-S. Liu, "Microfluidic Synthesis of Semiconducting Colloidal Quantum Dots and Their Applications," *ACS Applied Nano Materials*, Mar. 2019. Publisher: American Chemical Society.

[28] R. K. Kokal, A. R. C. Bredar, B. H. Farnum, and M. Deepa, "Solid-State Succinonitrile/Sulfide Hole Transport Layer and Carbon Fabric Counter Electrode for a Quantum Dot Solar Cell," *ACS Applied Nano Materials*, vol. 2, pp. 7880–7887, Dec. 2019. Publisher: American Chemical Society.

[29] R. Lin, X. Li, W. Zheng, and F. Huang, "Balanced Photodetection in Mixed-Dimensional Phototransistors Consisting of CsPbBr3 Quantum Dots and Few-Layer MoS2," *ACS Applied Nano Materials*, Apr. 2019. Publisher: American Chemical Society.

[30] P. Senellart, G. Solomon, and A. White, "High-performance semiconductor quantum-dot single-photon sources," *Nature Nanotechnology*, vol. 12, pp. 1026–1039, Nov. 2017.

[31] D. C. Unitt, A. J. Bennett, P. Atkinson, K. Cooper, P. See, D. Gevaux, M. B. Ward, R. M. Stevenson, D. A. Ritchie, and A. J. Shields, "Quantum dots as single-photon sources for quantum information processing," *Journal of Optics B: Quantum and Semiclassical Optics*, vol. 7, p. S129, June 2005. Publisher: IOP Publishing.

[32] D. Loss and D. P. DiVincenzo, "Quantum computation with quantum dots," *Physical Review A*, vol. 57, pp. 120–126, Jan. 1998. Publisher: American Physical Society.

[33] A. Vagov, M. D. Croitoru, V. M. Axt, T. Kuhn, and F. M. Peeters, "Nonmonotonic Field Dependence of Damping and Reappearance of Rabi Oscillations in Quantum Dots," *Physical Review Letters*, vol. 98, p. 227403, June 2007.

[34] A. Vagov, M. D. Croitoru, M. Glässl, V. M. Axt, and T. Kuhn, "Real-time path integrals for quantum dots: Quantum dissipative dynamics with superohmic environment coupling," *Physical Review B*, vol. 83, p. 094303, Mar. 2011.